Predicting the Elastic Modulus of 3D Braided Composite Tubes Using Geometrical Mapping Approach

Yi-bo Wang[1], Zhen-guo Liu[2], Long Hu[3], Zhe Wu[4].

[1]School of Aeronautic Science and Engineering, Beihang University(BUAA), Beijing 100191,R. P. China, Tel: +86-18066556110. E-mail address: wangyibo@buaa.edu.cn.
[2]School of Aeronautic Science and Engineering, Beihang University(BUAA), Beijing 100191,R. P. China, Tel: +86-13701323080. E-mail address: liuzg@buaa.edu.cn.
[3]School of Aeronautic Science and Engineering, Beihang University(BUAA), Beijing 100191,R. P. China, Tel: +86-18611690754. E-mail address: hulong0754@qq.com.
[4]School of Aeronautic Science and Engineering, Beihang University(BUAA), Beijing 100191,R. P. China, Tel: +86-10-51735605. E-mail address: wuzhe@buaa.edu.cn.

Keywords: 3-Dimensional reinforcement, Geometrical Mapping, Finite Element, Tubular unit-cell

ABSTRACT

The micro-geometry of three-dimensional (3D) braided tubular preform is more complex than that of rectangular one, for the macro-structure of yarns vary in different radial positions. This paper presented a FEM analysis for the 3D tubular braided composite tubes. Using Geometrical Mapping Approach, the tubular unit-cell model is established. This model reflects the change of the unit-cell macro-structure in radial direction. Then a FEM analysis of the established tubular unit-cell is presented. Deformation and stress distribution are obtained. Finally, the predicted longitudinal moduli were compared with the experiment results and the effects of some braiding parameters on the longitudinal moduli are discussed.

1 INTRODUCTION

Three-dimensional braided composites have received enormous attention due to their outstanding performances, such as high transverse strength, high shear stiffness, low delaminating tendency and high damage tolerance [1]. A number of analysis models have been developed that predict material behavior of various textile composites. On one hand, homogenization model [2-5] could forecast the elastic performance of the material precisely. Such models considered the composite as an assembly of homogeneous anisotropic elements. On the other hand, FEM (finite element method) models [6-9] considered the composite fibers and the surrounding matrix as distinct entities, which could deal with more complex problems which take interface and interactions between yarns into consideration [10].

For 3D tubular braided composite, some researchers have predicted longitudinal moduli of the braided tube using homogenization model [11-16]. While little focused on the FEM models [17]. In this paper, a tubular unit-cell model is established using the Geometrical Mapping Approach [10]. The unit-cell model consists of layers of sub unit-cell. Then the periodical boundary conditions and yarn element orientations are applied and a FEM analysis is conducted. Deformation and stress distribution are obtained. The predicted longitudinal moduli of this model were compared with the experiment results [14] and the effects of some braiding parameters on the longitudinal moduli are discussed.

2 GEOMETRICAL MAPPING APPROACH

The micro-structures of the tubular braids are the tubular braids are more complex than those of the rectangular ones. Yarn paths in tubular braids are spatial curves and the cross-sections of tubular yarns vary in different radial positions. In order to simplify the modelling method for tubular braids as well as combining currently wide-used rectangular unit-cell model. In this paper, the geometrical mapping approach was used. The rectangular unit-cell, which has same yarn topology with the target tubular unit-cell, was established firstly. And then the tubular model would be obtained by geometrical mapping from the rectangular model.

2.1 Rectangular unit-cell

To establish the tubular sub unit-cell, a rectangular unit-cell would be established firstly. Fig.1 is the interior unit-cell of the 3D 1×1 4-directional braided composite. h denotes the height, *A* denotes the width, the widths of the two edges in the bottom are equal, γ denotes the orientation angle of yarn, α denotes the interlacing angle which is equal to 90 degrees. There are 4 groups of yarn bundles and the 4 groups of paths interlace each other, the midline paths being approximately straight lines [18]. All the four orientation angles γ are equal, and

$$\gamma = \arctan(\sqrt{2}A / h) \tag{1}$$

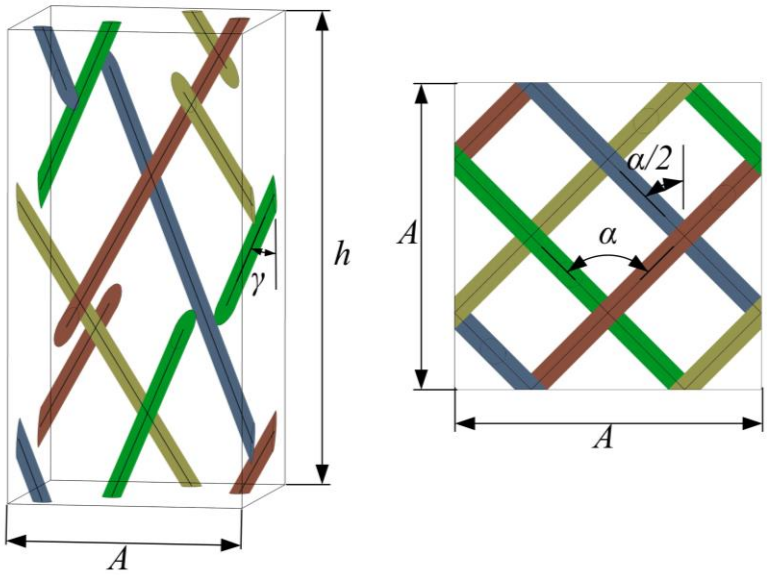

Fig.1 rectangular unit-cell of the 3D 1×1 4-directional braided composite

2.2 Tubular sub unit-cell

The size of the braiding carrier arrangement on the machine bed for tubular braid is denoted by *[M×N]*. M is the number of yarn carriers in circumferential direction and N the number in radial direction. The tubular unit cells according to the study in Ref. [19] can be typically divided into three categories: the sub unit-cell, the outer surface cell and the inner surface cell, as shown in Fig.2. Define m and n as

$$m = M / 2 \tag{2}$$

$$n = (N - 2) / 2 \tag{3}$$

Therefore one tubular unit-cell consists of n sub unit-cells, 1 outer surface cell and 1 inner surface cell.

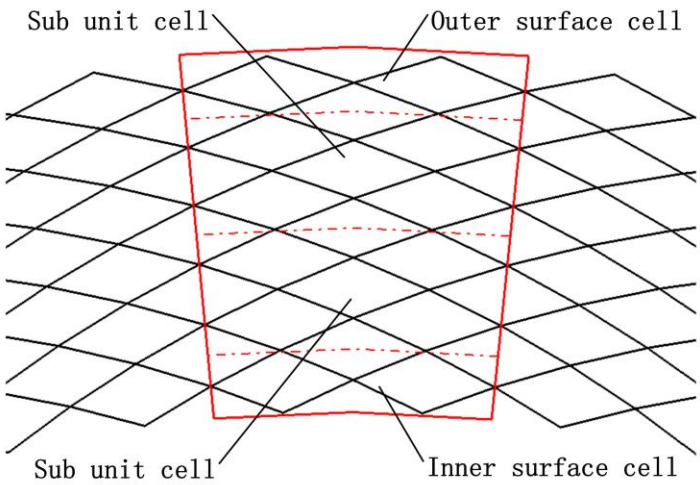

Fig.2 Tubular unit cell illustration

Although sub unit-cells have different sizes at different radial positions, they have analogous micro-geometry. Both 3D 4-step 1×1 rectangular and tubular preforms are braided by the same procedure, the yarn structure topologies of them are shown to be the same [11].

The tubular sub unit-cell, according to study in Ref. [19], is fan-shaped when observed in axial direction, as shown Fig.3. $\Delta\theta$ denotes the angular span of the tubular sub unit-cell. ΔR denotes the radial span of it. And according to Ref. [11], there are three important parameters to describe the micro-geometry of the 3D braided tubular preform: yarn braiding angle γ', radial interval distance Δr and interlacing angle α'.

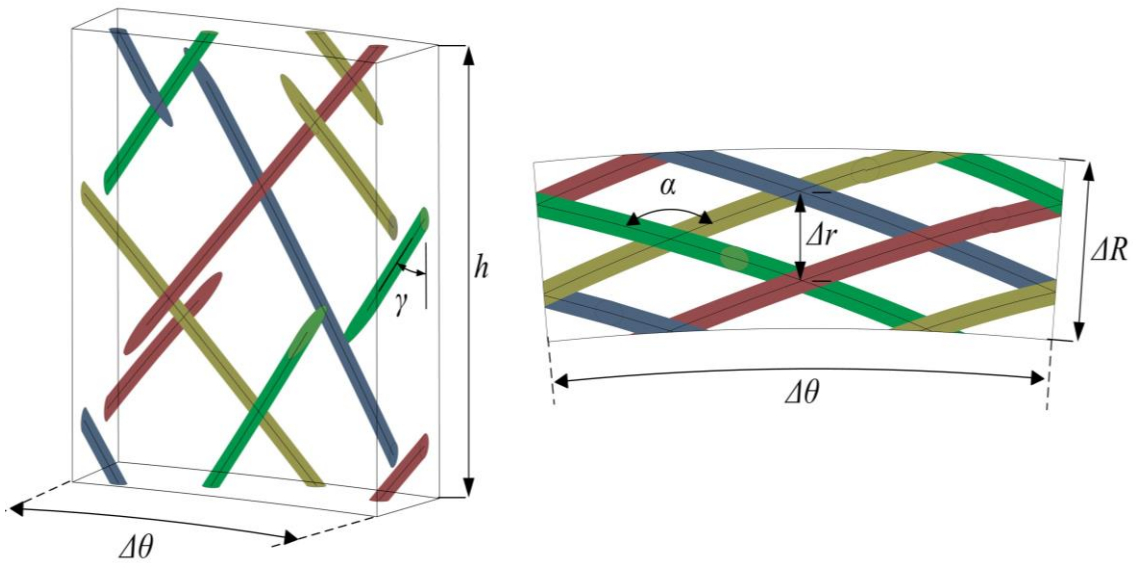

Fig.3 Tubular sub unit-cell of the 3D 1×1 4-directional braided composite

2.3 Geometrical Mapping relations

As discussed above, tubular preform of 3d braided composite have same topological features with the rectangular preform. And the tubular sub unit-cell as the representative volume element of a tube's preform has similar topological features with the rectangular unit-cell.

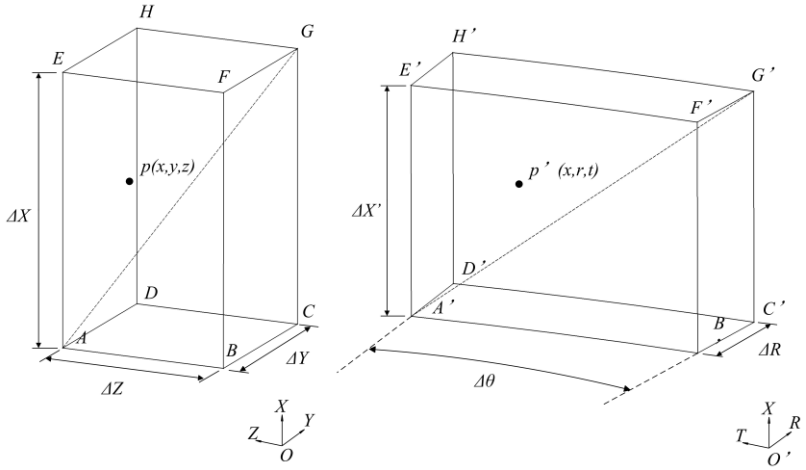

Fig.4 Mapping illustration

Define the Cartesian coordinate system O-XYZ and the polar coordinate system O'-XRT. The rectangular unit-cell ABCD-EFGH, which is a cuboid, is established in O-XYZ coordinate system. The tubular sub unit-cell A'B'C'D'-E'F'G'H' is established in O'-XRT coordinate system, as is shown in figure 4. P is any point of the rectangular unit-cell. P' is the corresponding point in the tubular unit-cell. P and P' have same topological features, so the mapping relations from P to P' is the mapping relations between the rectangular unit-cell and the tubular sub unit-cell. According to Ref. [10] the mapping relations between rectangular unit-cell and the tubular sub unit-cell is as follows:

$$\begin{cases} p'_x = p_x \\ p'_r = R(p_y) \\ p'_\theta = p_z \cdot \Delta\theta / \Delta Z \end{cases} \tag{4}$$

And the Function, $R(x)$, is the relations between p'_r and p_x, which in a differential equation form is written as:

$$\frac{dr}{dy} = \sqrt{\frac{r^2 \sin^2\gamma + 2\phi^2 \cos^2\gamma}{2r^2 - \phi^2 \sin^2\gamma}}, r(0) = R1 \tag{5}$$

In which, $\phi = \Delta Z / \Delta\theta$. ΔZ, equal to A mentioned in section 2.1, is the width of the rectangular unit-cell. $\Delta\theta$ is the angular span of the tubular sub unit-cell. And γ is the braiding angle of rectangular unit cell. R1 is the radius of the mandrel. Applying the initial condition $r(0) = R1$ to Eq.(5), one can get the relation between p'_r and p_y.

2.4 Geometrical Modelling

To establish the tubular sub unit-cell, a rectangular unit-cell is established firstly. Fig.5(a)(b) is the model of rectangular unit-cell established according to Ref.[18]. Then the rectangular unit-cell model is discretized and the coordinate of each discrete point is mapped using the mapping relations. Reconstructing the newly mapped point set, one can obtain the corresponding tubular sub unit-cell, as in Fig.5(c)(d). The mapped sub unit-cell model consistent with actual observations, Fig.6 is the CT scan results of the tubular braided composite. Yarns in the outer surface are more flatten than those in the inner surface.

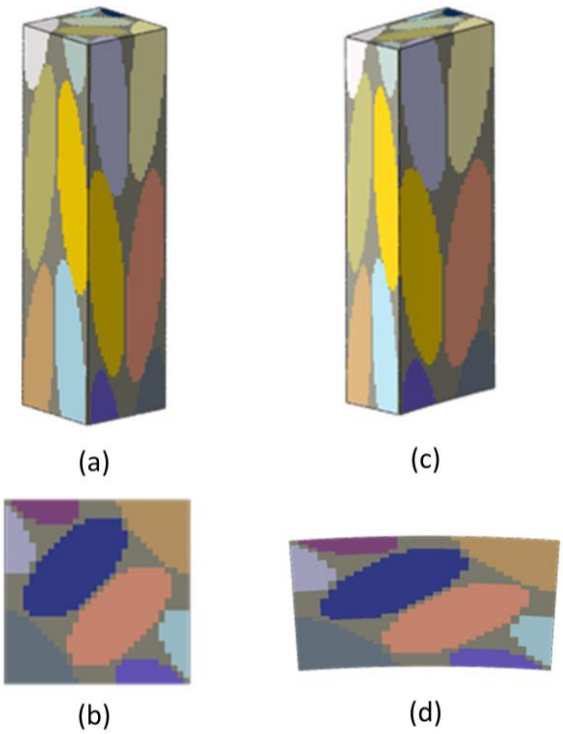

Fig.5 the Rectangular unit-cell and the Tubular sub unit-cell

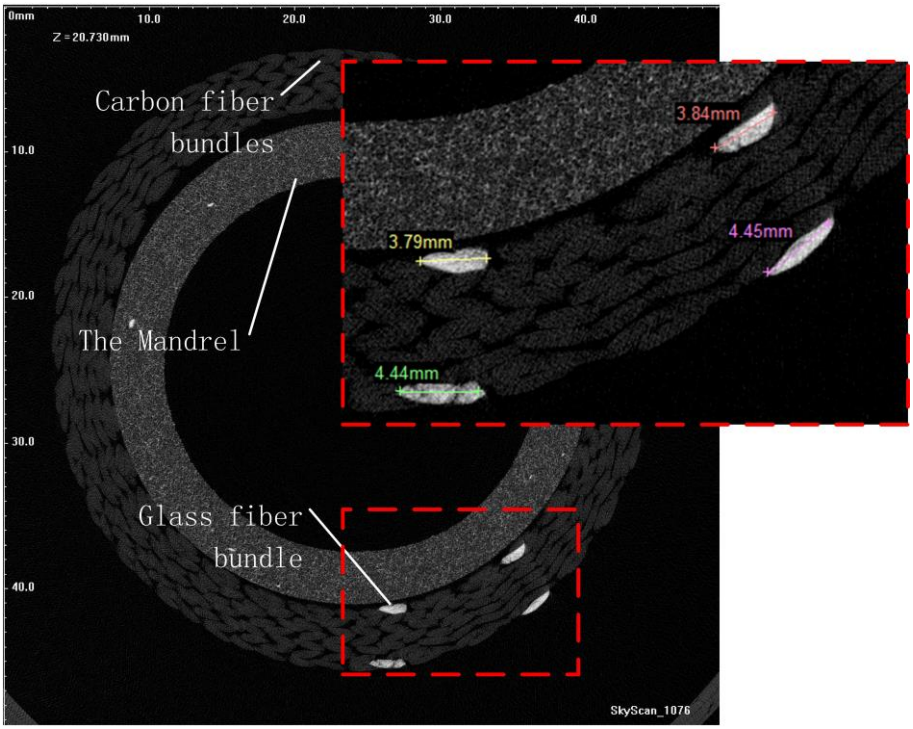

Fig.6 CT-scan results of the tubular braided composite

3 FEM ANALYSIS

3.1 Finite element model

A rectangular unit-cell model is established using TexGen which is open source software

developed at the University of Nottingham for geometric modeling of textile structures. According to Ref. [18], the relations of geometrical parameters of rectangular unit-cell can be expressed as follows:

$$\begin{cases} h = 8b / \tan\gamma \\ a = \sqrt{3}b / \cos\gamma \\ A = 4\sqrt{2}b \end{cases} \tag{6}$$

In equations (6), a and b are major and minor radii of the ellipse-assumed cross-section of braiding yarns, A is the width of the rectangular unit-cell. As can be seen, all the geometrical parameters of 3D rectangular unit-cell are expressed in terms of the free parameters h and γ. The value of h is equal to the pitch length which can be measured and γ can be obtained indirectly through measuring of the fiber volume fraction V_f , Ref. [10]. The relations between V_f and γ is as follows:

$$\frac{\tan^2\gamma}{\cos\gamma} = \frac{2N_f \pi d_f^{\,2}}{h^2 V_f} \tag{7}$$

In the equation (7), N_f is the number of monofil fibers included in one yarn bundle; d_f is the diameter of a single monofil fiber. N_f and d_f are determined by the braided yarns. For TC42S-12K carbon fiber product, N_f can be determined by the K-number (a thousand fiber is counted as 1 K) and d_f is 0.5μm [14].

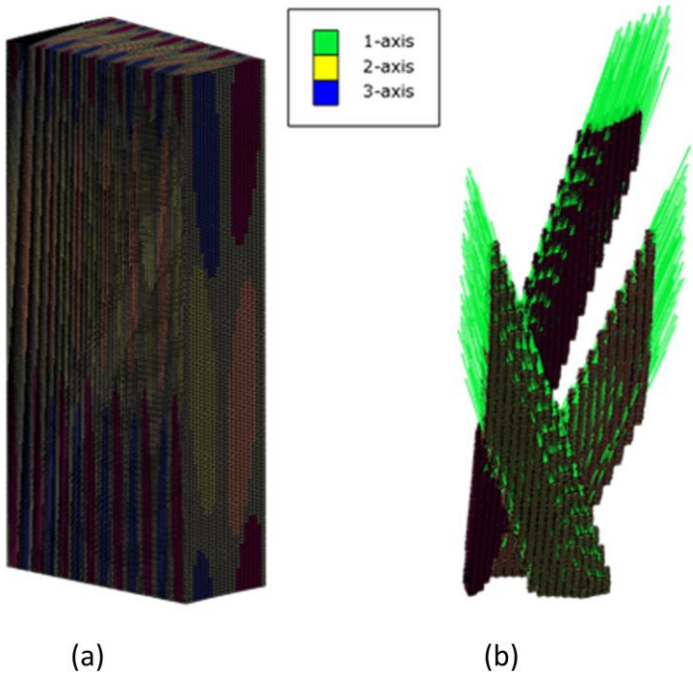

Fig.7 Finite Element Model of Tubular unit-cell and Element orientations

One unit-cell of 3d braided tubes contains n sub unit-cell, 1 outer surface cell and 1 inner surface cell, the tubular unit-cell. Here omitting the effect of surface cells, a unit-cell model with n layers of sub unit-cells was established, as in Fig.7. And n is determined by the size of the braiding carrier arrangement on the machine bed, as in section 2.2. Then using the Geometrical Mapping Approach, the corresponding tubular unit-cell was mapped. As illustrated in section 2.3, four parameters are needed for geometrical mapping: ΔZ ,γ, R1 and $\Delta\theta$. ΔZ and γ are determined by the rectangular unit-cell model. *R1* is the radius of the mandrel, which can be measured. $\Delta\theta$, the angular span of tubular unit-cell, can be calculated from the equation [10]:

$$\Delta\theta = \frac{2\pi}{m} \tag{8}$$

m is determined by the size of the braiding carrier arrangement on the machine bed, $[M \times N]$, as illustrated in section 2.2. The modelling parameters are shown in Table 1. In Table 1, $[M \times N]$, D_{out}, D_{inner}, θ_b, V_f are parameters of the specimens; h was calculated from $h = \pi D_{out} / 45 \tan\theta_b$ according to Ref. [14] and γ, A, $\Delta\theta$ are calculated from equations (6)-(8). The finite element models are shown in Fig.7(a).

Table 1 Modelling parameters of the tubular unit-cell

Parameters	A	B
$[M \times N]$- carrier arrangement	[90×15]	[90×15]
D_{out} -Outer diameter(mm)	41	31
D_{inner} -Inner diameter(mm)	30	15
θ_b - Outer surface braid angle	22.5	16.5
h - Pitch length(mm)	13.82	14.61
V_f - Fiber volume fraction(%)	59.1	60.1
$R1$ – Mandrel Radius(mm)	15	7.5
γ - Braiding angle of rectangular unit-cell(degree)	7.9	7.3
A - width of rectangular unit-cell(mm)	1.36	1.32
$\Delta\theta$ - Angular span of tubular unit-cell(degree)	11.25	11.25

3.2 Fiber yarn orientations

As in Fig.7(a), the model was discretized with voxel mesh. The yarn paths of three-dimensional (3D) braided tubular preform are more complex than the rectangular one. Fiber yarn paths in 3d tubular braided composite are spatial curves. To obtain the materials orientations, fiber yarn-path curves of the 4 group of yarns are mapped firstly. Then the materials orientations of each element in the yarn regions are obtained by centered difference of the yarn-path curves. As shown in Fig.7(b), the green lines are the directions of the material orientations of the yarn elements.

3.3 Boundary conditions

In general, composite materials are regarded as perfect periodic structures consisting of periodic array of unit-cells. There exists periodicity between the two opposite boundaries in circumferential direction and axial direction. The periodic boundary conditions should be applied to replicate its repeating nature. To ensure the displacement continuity conditions, such periodic boundaries are implemented to the corresponding boundaries:

$$\begin{aligned} u_x(p_1) - u_x(p_0) &= u_x(\mathrm{A'}) - u_x(\mathrm{E'}) \\ u_\theta(q_1) - u_\theta(q_0) &= u_\theta(\mathrm{A'}) - u_\theta(\mathrm{B'}) \end{aligned} \tag{9}$$

In Eq.(9), p_1 is an arbitrary point on boundary A'-B'-C'-D', p_0 is the corresponding opposite point on boundary E'-F'-G'-H'. q_1 is an arbitrary point on boundary A'-E'-H'-D' and q_0 is the corresponding opposite point on B'-F'-G'-C', as illustrated in Fig.4.

3.4 Deformation and stress distributions of unit cells

The advantage of the proposed analysis method is that the detailed information on the deformation and stress distribution of the tubular unit-cell under different loadings can be obtained. Fig.8 shows the deformation and stress distributions of the tubular unit-cell.

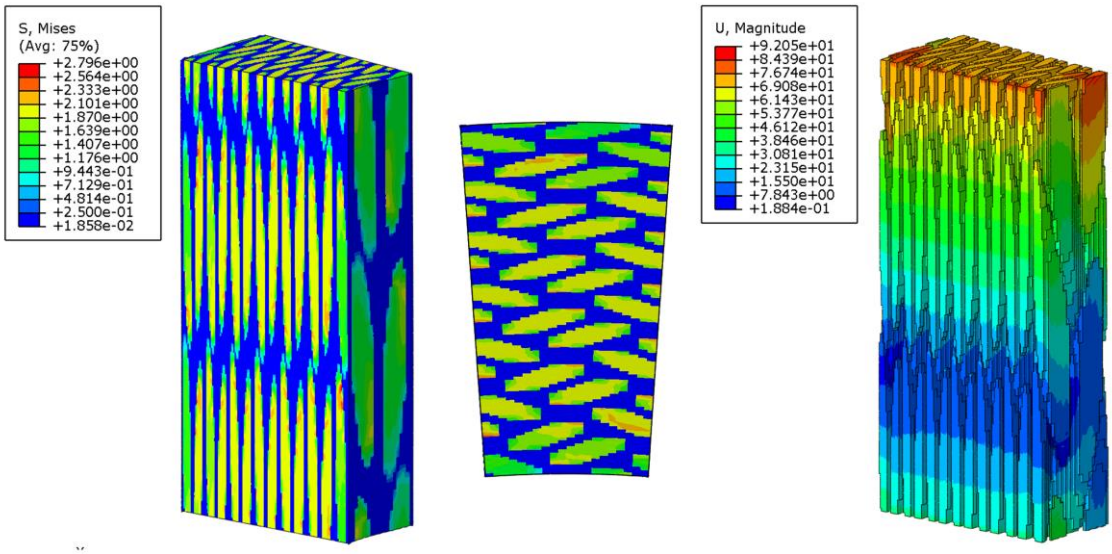

Fig.8 stress distributions and deformation

4 VALIDATION AND DISCUSSIONS

4.1 Verification of the Finite Element model

To validate the effectiveness of the finite element model, the predicted effective elastic moduli were compared with the experiment results from the compression test according to Ref. [14].The material properties and geometric parameters are listed in Tables 2 and 3. The predicted longitudinal moduli for the two specimens are close to the experiment results, as shown in Table 3, with errors within 10%. The errors may be caused by the omitting of the surface cells.

Table2 Materials properties

Epoxy resin (EMI-24)		**Fiber (TC42S-12K)**				
E_m (GPa)	G_m (GPa)	E_{f1} (GPa)	E_{f2} (GPa)	G_{f12} (GPa)	G_{f23} (GPa)	ν_{f12}
2.76	1.02	290	13.8	13.8	5.5	0.2

Table 3 geometry parameters and the comparision between FEM and experimental results

Specimen Ref. [14]	**Outer dia.**(mm)	**Inner dia.**(mm)	**Pitch length** (mm)	**Predicted Moduli** (GPa)	**Experiment results** (GPa)	**Error** (%)
A	41	30	13.8	74.5	6.91E+01	7.88
B	31	15	14.6	83.5	7.65E+01	9.13

4.2 The effect of pitch length on the longitudinal elastic moduli

The effect of pitch length on the effective elastic moduli of 3D four-step braided composite tube is studied for the Mandrel Radius *R1* = 17.5mm, Size of Machine Bed *[M×N]* = [64×6], Fiber Volume Fraction V_f = 60%, TC42S-12K/Epoxy. As depicted in Fig.9, the longitudinal modulus, E_{xx} increases with the increase in pitch length, which is attributed to fiber yarn orientations in the axial direction.

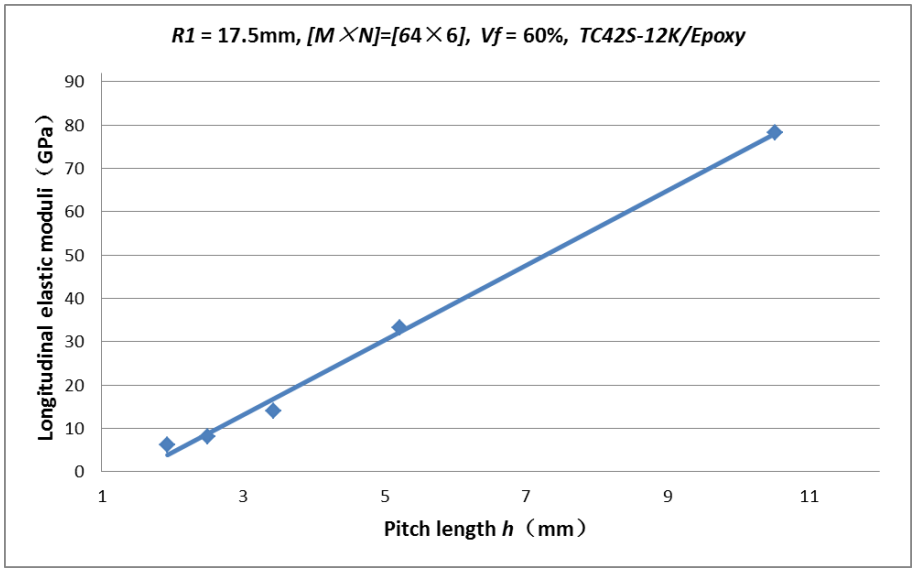

Fig.9 The effect of pitch length on the longitudinal elastic moduli

4.3 The effect of mandrel radius on the longitudinal elastic moduli

The effect of Mandrel Radius *R1* size on the effective elastic moduli of 3D four-step braided composite tube is studied for the Pitch Length h = 3.43mm, Size of Machine Bed $[M\times N]$ = [64×6], Fiber Volume Fraction V_f=50%, T700-12K/Epoxy. As depicted in Fig.10, the longitudinal Yong's modulus, E_{xx} decreases with the increase of Mandrel Radius *R1*, while the slope is reducing. With the increase of the Mandrel Radius, yarn orientations tend to the circumferential direction. So the pitch length decreases and the slope keeps reducing until the pitch length reaches the limits.

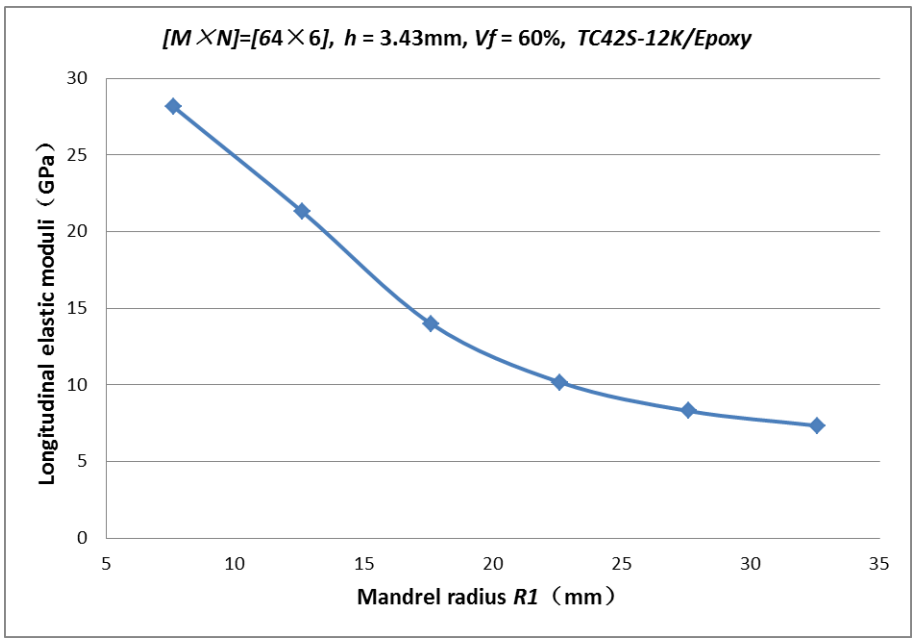

Fig.10 The effect of Mandrel Radius on the longitudinal elastic moduli

4.4 The effect of machine bed on the longitudinal elastic moduli

The effect of size of the braiding machine bed $[M\times N]$ on the effective elastic moduli of 3D four-step braided composite tube is studied for the Mandrel Radius *R1* = 17.5mm, Fiber Volume Fraction V_f

= 60%, TC42S-12K/Epoxy. As depicted in Fig.11, the longitudinal Yong's modulus, E_{xx} increases with the increase of the Circumferential Number *M*, while the rising slope in reducing. This is because with the increase of Circumferential Number *M*, yarns in the circumferential directions tend to squeeze, which reached the height limit of the pitch length.

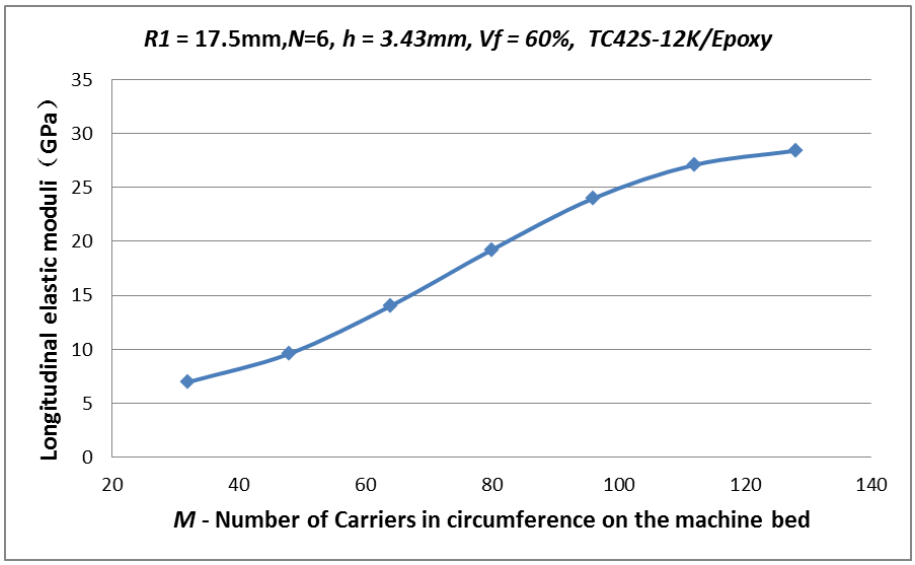

Fig.11 The effect of Circumferential Number on the longitudinal elastic moduli

As depicted in Fig.12, the longitudinal Yong's modulus, E_{xx} does not change significantly in different Radial Number *N*. And there exists a maximum. In fact, the increase of the radial number would increase the wall thickness of the tubular braids, which contains more tubular sub unit-cell in radial directions in microscopic structure, as seen in Fig. 2. In the rising stage of the curve, free-edge effect is the main factor. Because surface cell in proportion to the overall tubular thickness decrease with the increase of the sub unit-cells. In the descent stage, the new assembly tubular sub unit-cells are in a large radius positions. As seen in Fig.10, the elastic moduli of tubular braids decrease with the increase of the radial position. So the elastic moduli of the overall tube structure decreases.

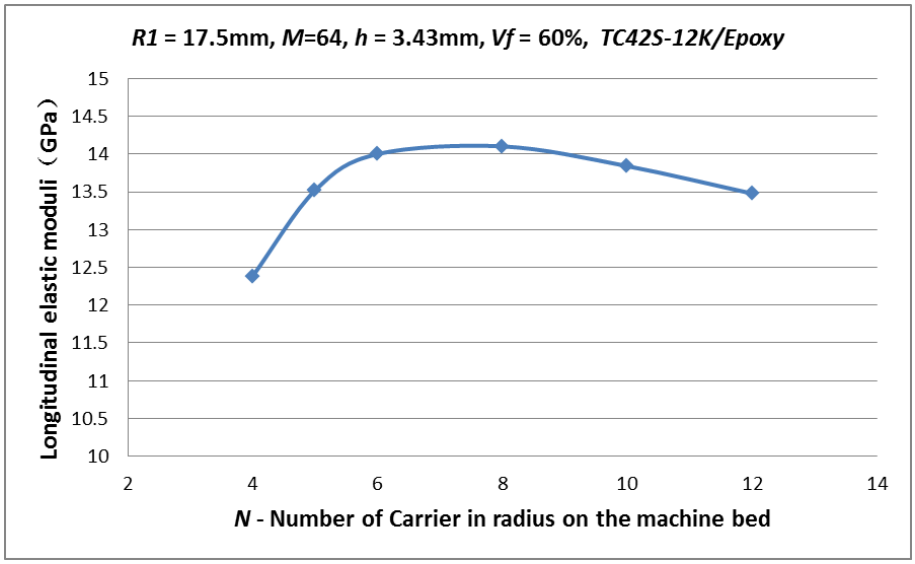

Fig.12 The effect of Circumferential Number on the longitudinal elastic moduli

5 CONCLUSIONS

This paper presented a FEM analysis method of 3D braided composite tube in the macro level. Stress distribution and deformations of the tubular unit-cell are obtained. The predicted longitudinal moduli are compared with the experimental results according to Ref. [14], and the predicted errors are within 10%. Then, variation of geometrical parameters is used to study the effect of the braiding parameters on the mechanical properties. The longitudinal Young's modulus increase with the increase of pitch length; and the longitudinal Young's modulus reduces with the increase of the mandrel radius and the slope reduces when the pitch length approaches its low limit; the size of the machine bed affect the longitudinal Young's modulus a lot; the longitudinal Young's modulus increased with the increase of the circumferential number on the machine bed and the rising slope reduces when the pitch length approaches its height limit; the effect of the radial number is not significantly, but there exists a maximum. Reasonable calculation results are obtained and it is shown that geometrical mapping was an effective modelling approach for tubular unit-cell. Some of the tubular model can be obtained by geometrical mapping from the rectangular model, which has the same yarn topological structures. Further to validate the feasibility of this analysis method, additional experiments and mechanics simulation are needed.

REFERENCES

[1] Liu Z G. Study on Comparison of Manufacturing Methods of High Performance Composites Pipes and Application of 3D Braiding Technology. Journal of Materials Engineering 2009, 2, pp.109-113.
[2] Miravette A. 3-D textile reinforcements in composite materials. Cambridge: Woodhead Publishing Limited, 1999.
[3] Ko F K. Tensile strength and modulus of a three dimensional braid composite. Proceedings of the 7th Conference on Composite Materials: Testing and Design. Philadelphia, PA: ASTM STP 893, USA, 1986, pp. 392–403.
[4] Yang, Jenn-Ming, Chang-Long Ma, and Tsu-Wei Chou. Fiber inclination model of three-dimensional textile structural composites. Journal of Composite Materials 1986;20(5):472-484.
[5] Wu DL, Shen HR. Behavior of textile structural composites. Changsha: National University of Defense Technology Press, 1998. pp. 63–129.
[6] Chen L, Tao X and Choy C. On the microstructure of three-dimensional braided performs. Composite Science and Technology 1999 59(3), pp.391–404.
[7] Lu Z X, and Liu Z G. Numerical prediction of three-dimensional textile composite material strength. Journal of Beijing University of Aeronautics and Astronautics 2002;28(5), pp. 563-565.
[8] Fang GD, Liang J, Lu Q, Wang BL and Wang Y. Investigation on the compressive properties of the three dimensional four-directional braided composites. Composite Structure 2011;93(2):392–405.
[9] Zhang, F, et al. A new scheme and microstructural model for 3D full 5-directional braided composites. Chinese Journal of Aeronautics 2010;23(1), pp. 61-67.
[10] Yi-bo Wang, Zhen-guo Liu, Nian Liu, Long Hu, Yu-chen Wei, Jia-jun Ou. A new Geometric Modelling Approach for 3D Braided Tubular Composites base on Free Form Deformation. Composite Structures 136 2016 pp.75–85
[11] Wang Y Q, Wang A S D On the topological yarn structure of 3-D rectangular and tubular braided performs. Composites Science and Technology 1994;51(4) , pp. 575-586.
[12] Wang Y Q, Wang A S D. Yarn structures in 3-D braided composites due to complex shape change. American Society of Mechanical Engineers 1995;56:151-166.
[13] Wang Y Q, Wang A S D Spatial distribution of yarns and mechanical properties in 3D braided tubular composites. Applied Composite Materials 1997;41, pp. 121–132.
[14] CL Hwan, KH Tsai, WL Chen, et al. Predicting the elastic moduli of three-dimensional (four-step) braided tubes using a spatial spring model. Journal of Composite Materials 2012;0(0) , pp. 1–10.
[15] Zhi-Min Li, Hui-Shen Shen. Postbuckling analysis of 3D braided composite cylindrical shells under torsion in thermal environments. Composite Structures 2009;87(3) , pp. 242-256.
[16] Wensuo Ma, Jianxun Zhu and Yun Jiang. Studies of fiber volume fraction and geometry of

variable cross-section tubular 3D five-direction braided fabric. Journal of Composite Materials 2011;46(14) , pp. 1697-1704.

[17] X K Sun. Micro-geometry of 3-D braided tubular preform. Journal of Composite Materials 2004;38(9) , pp. 791-798.

[18] C Zhang, X Xu. Finite element analysis of 3D braided composites based on three unit-cells models. Composite Structures 2013;98(0) , pp. 130–142.

[19] Lee, W., Kim, J.H., Shin, H.-J., Chung, K., Kang, T.J., Youn, J.R. Constitutive equations based on cell modeling method for 3D circular braided glass fiber reinforced composites. Fibers and Polymers 2003;4(2) , pp. 77-83.